Phasing ELTs for Adaptive Optics: Preliminary results of a Comparison of techniques

Venice 2001
Beyond Conventional Adaptive Optics

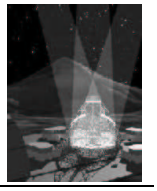

Achim Schumacher[a], Luzma Montoya[b], Nicholas Devaney[a], Kjetil Dohlen[b] and Philipe Dierickx[c]

[a]Instituto de Astrofisica de Canarias, GTC Project, 38200 La Laguna, Tenerife, Spain,
[b]Laboratoire d'Astrophysique de Marseille, 2 Place Leverrier, 13248 Marseille Cedex 4, France,
[c]European Southern Observatory, Karl Schwarzschildstr. 2, D-85748 Garching bei München, Germany

ABSTRACT

There is no doubt that the future telescopes of diameter more than 10m, dubbed 'ELTs', will employ segmented mirrors. The performance of these telescopes may be severely limited by discontinuities in the wavefront, caused by segmentation errors such as segment piston, tip-tilt, figure errors and edge effects. These will particularly affect AO performance, and it is therefore of interest to know what techniques are available to reduce these errors, and what performance can be expected of them. In the framework of a Research and Training Network on Adaptive Optics for ELTs, funded by the European Commission, we are in the process of evaluating the performance of various piston measurement techniques which are either in use on current segmented telescopes, or which have been proposed. In this article we present an overview of these phasing techniques and the performance criteria we will use to compare them. We give detailed results on our study of one particular technique, the Chanan narrow-band phasing technique, which is employed on the 10m Keck telescopes and will also be employed in a modified form on the 10m Gran Telescopio Canarias (GTC). We have developed a new algorithm for extracting the phase information and show that this leads to improved performance. We show that the technique can work with sufficient precision on telescopes as large as 100m.

1. INTRODUCTION

In addition to the usual optical errors associated with monolithic telescopes, segmented mirror telescopes present other errors due to segment misalignment. In general, the segments have six degrees of freedom; translation along two axes in the plane of the segment, rotation about a vertical axis, rotation about two horizontal axes (tip and tilt), and translation along the vertical axis (piston). Undesired motion in any of these degrees of freedom will give rise to departure from the ideal mirror shape and hence affect the wavefront quality. Movement in piston or tip-tilt generally produces wavefront discontinuities. Movement in the first three degrees of freedom is restricted by attachment to the primary mirror cell and will not be considered further here. The segments usually have three actuators each, allowing the segment to be positioned in tip, tilt and piston. The effect of these errors on long-exposure image quality has been examined elsewhere (Bello et al., 2000) and the effect on diffraction-limited images has also been presented (Zeiders, 1998). As it is planned that practically all ELT observations will employ adaptive optics, we are particularly concerned with the effect of these errors on diffraction-limited images.

We will consider piston and tip-tilt separately. The effect of random segment piston errors on Strehl ratio depends on the statistics of the piston errors. However, in the limit of small piston errors, the average Strehl ratio is given by (Yaitskova, 2000)

$$< S > \approx 1 - \sigma^2 \left(1 - \frac{1}{N}\right), \quad (1)$$

where N is the number of segments and σ^2 is the variance of the segment piston errors. The effect is larger as the number of segments increase, and for ELTs the Strehl ratio can be approximated by $1 - \sigma^2$. In the near infrared, this expression may be taken to imply quite relaxed values of piston. However, since piston will be only one term in a long list of wavefront error sources, it will in fact be necessary to control it precisely. For example, a Strehl requirement of 0.95 at a wavelength of 1.25 microns implies an accuracy of 44nm in the segment piston control (note that in this article piston values are referred to the wavefront, values at the mirror are a factor of two smaller). Of course, if it is hoped to carry out

Adptive Optics at visible wavelengths, then the piston errors will have to be small. For example, a Strehl ratio larger than 0.9 at a wavelength of 0.55 microns implies piston errors less than 25nm (12.6nm at the mirror).

In the case of small tip-tilt errors, the Strehl ratio is given by (Yaitskova, in prep.)

$$< S > \approx 1 - \sigma_\theta^2 \cdot \gamma, \tag{2}$$

where σ_θ^2 is the variance of the tip-tilt angle and $\gamma = 5/36$ in the case of hexagonal segments. For example, for a segment dimension of 2m, a Strehl ratio greater than 0.95 at a wavelength of 1.25 microns corresponds to rms tip-tilt errors of less than 54 nrad (0.011 arcsec). Tip-tilt errors can be measured with high precision using, for example, a Shack-Hartmann wavefront sensor.

This discussion assumes that the AO system will not correct any of the wavefront error introduced by segment misalignment. In fact, AO will always provide partial correction, even if the AO system is not specifically designed to do so (Gavel, 1997). This is especially true in the case of high-order AO. For low-order AO where there are not many subapertures per segment, it would be advantageous to choose the geometry of the AO wavefront sensor so that there are subapertures which cross segment edges in a regular way (Bello, 2000). In general, it is necessary to carry out numerical simulations in order to accurately determine the performance of a given AO system in the presence of segment misalignments. However, in the absence of simulations, expressions (1) and (2) may be taken as pessimistic estimators of the effect of piston and tip-tilt on the Strehl ratio.

A now classical method for phasing segmented mirrors is that implemented in the Keck telescope. Individual segment tilt and piston are adjusted in closed loop using position actuators, the error signal being provided by capacitive sensors measuring inter-segment steps. Periodic calibration of these sensors is required, and a number of convenient techniques have been developed by Chanan et al. (2000), and will be further discussed in Sect. 3. The loss of operational time implied by periodic calibration is moderate; at the Keck, the reported duration of a calibration run is less than an hour and the periodicity is counted in weeks. Accuracy is deemed sufficient for seeing-limited performance. In view of the technological progress made since the design of the Keck telescopes, substantial improvements in sensor characteristics should allow a further reduction of the operational load implied by this methodology, and Chanan indicated that the technique could readily be extrapolated to a large number of segments (Chanan, 2000).

In the case of Extremely Large Telescopes, for which near-diffraction limited performance is mandatory, it remains to be established whether this technique can meet the requirements. In addition, in view of the large number of segments – up to several thousands – reliability considerations may imply that the frequency of calibration or cross-checks has to be increased. It is in this context that this article is presented.

Quite a number of alternative calibration techniques have been proposed over the last few years. Our long-term purpose is to assess the potential performance of each method, devise and perform laboratory and on-sky experiments for the most promising ones, and eventually establish a phasing methodology for an adaptive, Extremely Large Telescope such as the 100-m OWL. This article covers a brief overview of existing or proposed on-sky calibration methods, and provides preliminary simulation results.

2. OVERVIEW OF TECHNIQUES

There are several considerations to be taken into account when comparing segment alignment techniques. The precision of the technique should of course be better than the alignment specification, while the range should cover the expected errors due to thermal and gravitational deformations, sensor drift etc. It would also be desirable for the technique to have sufficient range to align segments after they have been installed. The measurement should be fast so as not to take up useful observing time. Even if it can be carried out in parallel with observation, the time taken should be short compared with typical active optics timescales (minutes). The technique should not require interaction with the telescope (e.g. stepping the segments). Finally, the comparison should evidently include cost and operational complexity.

Several approaches to segment alignment can be found in the literature. In order to correctly position a segment, it is necessary to determine the three dimensional position of three non-colinear points on the segment surface. The approaches to determining segment position can be grouped as follows (Glecker, 1991): (i) absolute position (ii) relative piston and absolute tip-tilt and (iii) relative piston and relative tip-tilt.

The absolute position of the segment in three dimensions can be obtained using techniques such as absolute distance interferometry. The practical implementation would be complex and the accuracy in measuring (for example) the distance from the segments to a point on the secondary mirror would be several microns at best.

The absolute tip-tilt of the segments can be found using a Shack-Hartmann wavefront sensor with a single subaperture per segment. If an AO system is operating, the segment tip-tilt could be determined by low-pass filtering applied to subapertures falling within segments. It would be necessary to know the orientation of the subaperture array with respect to the segmentation pattern at all times. In principle, the absolute tip-tilt can also be determined by other techniques which would not require part of the light to be diverted to a wavefront sensor e.g. using a laser scanner and small reflectors or holographic optical elements on the segments. However, it would appear more practical to employ wavefront sensor information from the AO system or from a dedicated sensor which can be deployed in the field of view. Relative piston can be sensed either optically or using capacitive or inductive edge sensors. The Keck telescope employs capacitive edge sensors (Minor, 1990), while inductive edge sensors have been proposed for the CELT telescope (Nelson, 1999). In either case, optical calibration of these sensors will be required on a regular basis.

Finally, relative piston and relative tip-tilt measurement can be carried out using two edge sensors on the segment edges. This is the strategy employed at the Keck telescope. It is not sensitive to modes which do not give rise to edge discontinuities e.g global tilt, piston or Śfocus modeŠ, in which the segments move in piston and tilt to give rise to a primary mirror defocus. These modes can be determined by low-order wavefront sensing. Again, the edge sensors need to be calibrated optically from time to time.

The optical techniques which are either employed or proposed to measure relative piston will be outlined in the remainder of this section (see also Owner-Petersen et al. (1999)).

2.1. Wave-Optics Shack-Hartmann Sensing

This technique was developed to optically phase the Keck telescopes. It is based on a wave-optics generalization of Shack-Hartmann wavefront sensing. It will be considered in detail in this article (Section 3).

2.2. Curvature Sensing

Curvature sensing is based on measuring the difference in intensity between images obtained equal distances before and after the telescope focus, and is employed in several adaptive optics systems (Roddier, 1991). It has been proposed that curvature sensing can be used to detect piston errors (Rodriguez-Ramos,1996). Cuevas (2000) has shown that the curvature signal does indeed contain information on relative pistons. When the extra-focal distance is large, the relative piston between two segments gives rise to a 'double-delta' function in the curvature signal along the segment boundary. The amplitude of the delta functions is proportional to the relative piston. In the approach of Rodriguez-Ramos & Jimenez (Rodriguez-Ramos, 1996), the extra-focal distance is small and the signal dependence on relative piston is non-linear. An iterative algorithm is therefore used to extract the piston information. Chanan (Chanan, 2000) has used a curvature-type sensor to measure piston errors at the Keck telescope. In his experiments, he obtained de-focused images on an infrared camera operating at a wavelength of 3.3 microns. He determined the piston error on a segment-by-segment basis by comparing the curvature signal with numerical simulations of the curvature signal corresponding to different piston errors in a single segment. He reports an accuracy of $\approx$40nm.

2.3. Interferometry

Relative piston errors can be measured using different interferometric techniques, such as Mach-Zehnder (Angel, Jacobsen, 1994) or shearing interferometry (Horton, 1990). In general, white-light interferometry is necessary in order to identify zero piston error, while narrow-band interferometry is required to increase precision. In the Mach-Zehnder scheme, light from a star is divided between the two arms of the interferometer; the light is passed through a pinhole on one arm and then re-combined with the light in the other arm. If used with adaptive optics, the pinhole size can be diffraction-limited. The technique can measure piston errors for all segments simultaneously. In the radial shearing approach proposed by Horton (1990), the image of one segment is magnified and made to interfere with light from surrounding segments. In the absence of adaptive correction, the interference fringes will be randomly (and rapidly) distorted by atmospheric turbulence, and this represents a fundamental limitation of these techniques. Dohlen (1998) proposed making interferometric measurements simultaneously at two wavelengths in order to remove the 2π ambiguities in the piston measurements. It has also been proposed to mount a Michelson interferometer on a robotic arm which positions the interferometer in front of the segment edges (Arasa, 2000). This technique has the advantage of being able to operate in the daytime, and therefore does not use any useful observing time. The interferometer needs to include active fringe stabilization in order to cancel the effect of mechanical vibrations.

2.4. Pyramid Wavefront Sensing

It has recently been suggested that pyramid sensing could be used for piston sensing. This idea has been examined using simulations and the results are presented elsewhere in these proceedings (Esposito & Devaney).

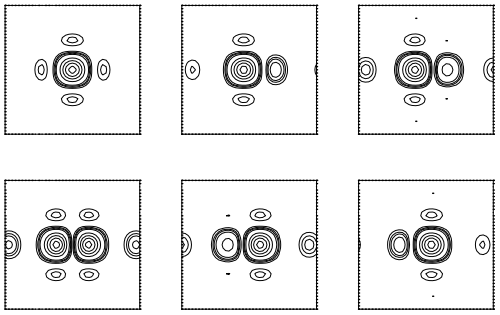

Figure 1. Simulated diffraction patterns for a split squared subaperture with wavefront step δ between the two halves given by $k\delta = 0, 2\pi/6, 4\pi/6, ..., 10\pi/6$.

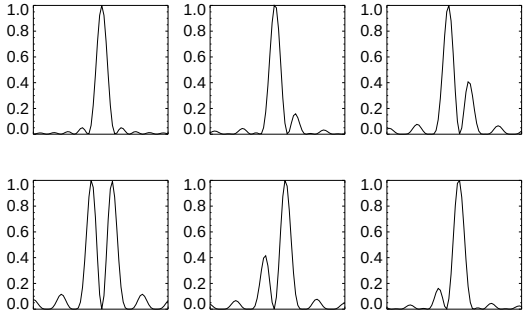

Figure 2. x-projection of images of Fig. 2

2.5. Phase Diversity

In phase-diverse wavefront sensing, pairs of in-focus and out-of-focus images are recorded. The amount of defocus is small and precisely known. An iterative technique is used to find the pupil aberrations which best match the measured data. This is similar to phase retrieval, but the de-focused image provides extra constraints on the solution. It was predicted that it should be possible to use this technique to determine piston errors (Paxman, 1988). An experiment was carried out at the Keck telescope, but the results were inconclusive. This may be due to the fact that the seeing was poor and the stellar reference source, which was supposed to be point-like, was in fact resolved by the telescope (Lofdahl, 1998). They propose to repeat the experiment in parallel with operation of the Keck adaptive optics system.

3. THE CHANAN NARROW-BAND ALGORITHM APPLIED TO ELTS

This technique is the first we have investigated in detail. It is based on a Shack-Hartmann-type wavefront sensor, where the lenslet array is preceded by a mask at the position of the exit pupil that defines small subapertures at the center of each of the intersegment edges. In the case of the Keck telescopes, these subapertures are circular; in this paper we refer to square subapertures as will be used at the GTC (Devaney, 2000). The size of the subapertures is chosen to be smaller than the average Fried parameter, r_0, of approximately 20cm at a wavelength of 500nm. At the Keck and at the GTC this size is 12cm with respect to the primary mirror.

3.1. Description of the Algorithm to Extract the Phase

In this section we will concentrate on the algorithm applied to extract phase information from a single intersegment edge step (or piston step). The original Chanan narrow-band technique (Chanan, 1998) is described and compared to a modified algorithm. Both techniques exploit the diffraction pattern produced by a small intersegment subaperture and monochromatic light from a bright stellar source. The resulting simulated diffraction patterns for various piston steps are shown in Fig. 1, and their projection on the x-axis in Fig. 2. The two algorithms under comparison differ in the way they make use of these images.

In the Chanan approach, an image taken from a subaperture with unknown piston step is compared to a set of 11 simulated images like those of Fig. 1. The real piston step is somewhere between the piston steps of the two most similar images. The degree of similarity is determined by calculation of a correlation coefficient; a finer resolution than the piston step difference between two templates ($\lambda/11$ at the wavefront (WF)) is achieved by quadratic interpolation of the correlation coefficients. For improved accuracy the primary mirror segments are stepped though 11 piston values spanning $\lambda/11$ (WF) using the segment actuators.

We propose a new approach which is based on extracting a single characteristic value from each simulated image related to the piston step, and then calculating a calibration curve. One possible characteristic value, which will be applied here, is the ratio between the two main peaks in the diffraction pattern (see Fig. 2). We will refer to this technique as the peak ratio technique (See also (Bello, 2000)). Defining the peak ratio as $PR = Max(right\ peak)/Max(left\ peak)$ we obtain the calibration curve shown in Fig. 3. In this figure the calibration points obtained from the simulation are plotted together with a fitted polynomial of third degree to (the logarithm of) these points; it represents the data with sufficient accuracy. The coefficients of this polynomial are used as calibration data. For a given subaperture image, the peak ratio is calculated and processed with the calibration data in order to obtain the required piston step.

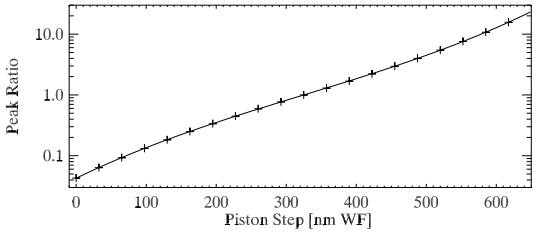

Figure 3. Peak ratio calibration curve ($\lambda = 650$nm).

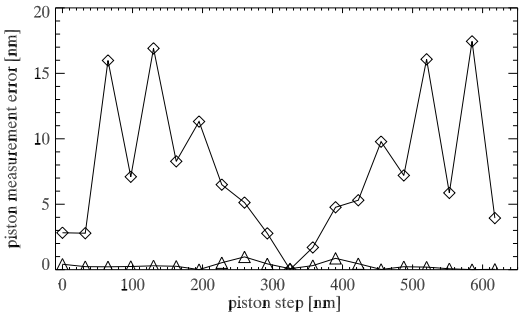

Figure 4. Measurement precision of the Chanan (diamonds) and the peak ratio (triangles) technique under perfect conditions.

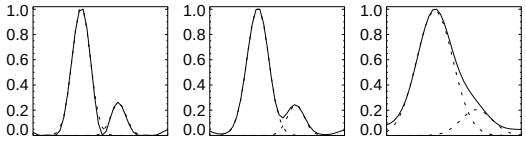

Figure 5. 1d-diffraction patterns at various seeing conditions r_0(500nm)=∞, 16cm, 6cm.

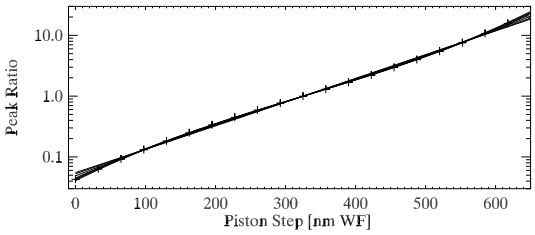

Figure 6. Peak ratio calibration curves at various seeing conditions down to r_0(500nm)=8cm (λ=650nm).

The resulting precision under perfect conditions of the Chanan technique (without stepping the segments) and of the peak ratio technique are plotted in Fig. 4. The precision of the peak ratio technique is only limited by the validity of the polynomial fit to the calibration data and by calculation roundoff errors, whereas the original Chanan technique shows an intrinsic error of up to 18nm. The performance under non-perfect conditions is discussed in the following sections. Possible sources for the intrinsic error of the original Chanan technique are the following: (i) To calculate the correlation coefficients, all images first have to be re-registered, so that the centroids coincide exactly with the array center, and not just to within the nearest pixel. (ii) The correlation coefficients do not exactly show a quadratic dependence. In (Chanan, 1998) a deviation of up to 0.7% between the coefficient and its quadratic approximation is stated. (iii) The process of calculating the correlation coefficient itself could be an error source. Since we used our own analysis code, it is possible that the code used at Keck is further optimized and shows less intrinsic errors.

It is possible to extract the maximum values of the peaks even in bad seeing conditions or with relatively high photon noise. In Fig. 5 the resulting PSF for various seeing conditions and a fixed piston step of $\lambda/4$ are plotted (straight line). As the seeing gets worse, the binary structure gets less distinct. But even in the case of barely having a binary structure it is still possible to extract the maximum heights of the two peaks involved. Fitting the sum of two gaussians to the PSF will yield the results shown in Fig. 5 (dotted lines). With this method it is possible to obtain a result for Fried parameters as small as $r_0 \approx 6$cm at 650nm. As is shown in Fig. 6, the calibration curves obtained for different seeing conditions differ slightly, leading to measurement errors as discussed in Sect. 3.2. This Gaussian fit method is also suitable for the case of having photon noise as discussed in Sect. 3.3. An important advantage of the Gaussian fit method is the fact that it provides not only the values of the two peak heights, but also an estimation of their uncertainties. Knowing the precision of each piston step measurement allows us to perform a weighting when calculating the segment piston values from all measured subaperture piston step values, as described in Sect. 3.4.

Both the Chanan and the peak ratio technique result in a useful range which depends on the wavelength used. The maximum unambiguous piston step is $\pm\frac{\lambda}{2}$ at the wavefront. The maximum deviation from the mean value of the segment pistons is then $\pm\frac{\lambda}{8}$ at the mirror. In the case of $\lambda = 650$nm this means that the segments have to be already aligned to better than 162nm. It is therefore convenient to take another measurement at a different wavelength in order to avoid the ambiguities. If $\lambda_1 = 650$nm and $\lambda_2 = 850$nm then the range is about 10 times greater.

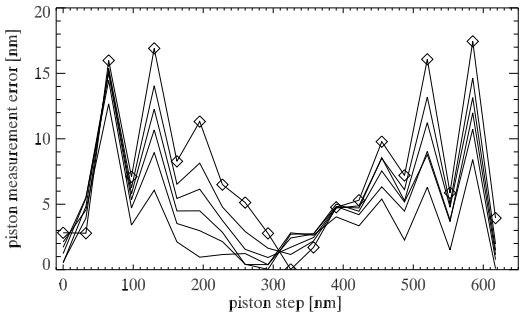

Figure 7. Measurement precision of the Chanan technique under various seeing conditions. Diamonds represent data with perfect seeing conditions.

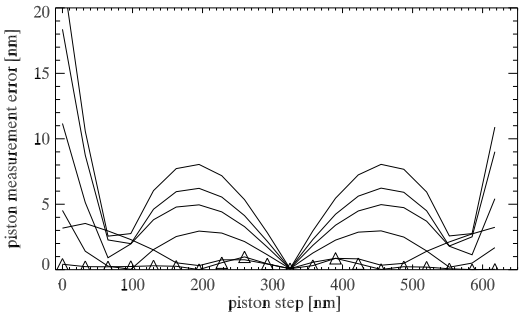

Figure 8. Measurement precision of the peak ratio technique under various seeing conditions, using calibration data obtained for best seeing conditions. Triangles represent data with perfect seeing conditions.

3.2. Performance as Function of Seeing

As described in Sect. 3.1 and shown in Fig. 5 the shape of the diffraction pattern changes with the seeing conditions. The way this affects the measurement precision depends on the method chosen to extract phase information. At the Keck telescopes, only 11 images at perfect seeing conditions are simulated and compared to the real image under investigation. Surprisingly, the original Chanan technique works better when seeing gets worse, as can be seen in Fig. 7. In the peak ratio technique worse seeing conditions will produce a greater peak ratio error due to a systematic error in the gaussian fit. The resulting measurement errors for various seeing conditions are shown in Fig. 8. The precision is greatly affected by the seeing condition. However, since the error of the gaussian fit is systematic, one can correct for it. Calculated calibration curves for various seeing conditions are shown in Fig. 6. The real seeing condition can be estimated from the width of the fitted peaks and one can apply the corresponding calibration curve. The resulting piston step measurement error is then almost reduced to its value at perfect conditions, as can be seen in Fig. 9.

3.3. Performance as Function of Magnitude

In this section we will calculate the stellar magnitude required to phase the mirror using the narrow-band technique with the peak-ratio algorithm. The limiting stellar magnitude will depend on the number of photons required to measure the piston errors with the specified accuracy. The magnitude of a star is related to the number of photons arriving at the detector as follows:

$$n = \eta t A \epsilon 10^{-0.4\,M} \Delta\lambda \tag{3}$$

where ϵ is the system efficiency, t is the exposure time, A is the collecting area, η is the number of photons per cm^2 per nm from a zero magnitude star, $\Delta\lambda$ is the bandwidth, and M is the magnitude of the star.

Figure 10 shows the error in the piston measurement for different photon levels. The given error is the standard deviation of 360 random simulations at different piston steps – it turned out that in the case of photon noise the gaussian fit error does not depend on the piston step value. In order to keep the standard deviation due to photon noise in the piston step measurement below 5nm, approximately 10000 photons per subaperture are required. Although 5nm seems to be small, one should bear in mind that this is a standard deviation and single measurements may be affected by higher errors. From simulations of whole mirrors we found that 10000 photons per subaperture will give stable results at all times.

Table 1 shows the limiting stellar magnitude and the corresponding required accessible field to find such a star with a probability of 90% for different photon levels at the North and South Galactic Poles. Here we assumed the following values: ϵ=0.8, which is the product of the transmission from the top of the atmosphere to the detector, and the detector quantum efficiency, t=60 seconds, which is typical of active optics timescales, A=144 cm^2, corresponding to square subapertures with a side length of 12cm, $\Delta\lambda$=10 nm, and η(650nm)=8730 $cm^{-2}nm^{-1}$. The required field of view (FOV) can be obtained from the probability P of finding at least one star within a given radius, r, on the sky. Since the distribution of stars on the sky follows Poisson statistics, P is given by:

$$P = 1 - e^{-r^2 \nu \pi / 3600^2} \tag{4}$$

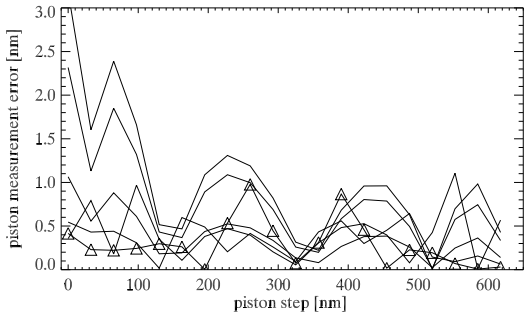

Figure 9. Measurement precision of the peak ratio technique under various seeing conditions, using the calibration data corresponding to the actual seeing condition. Data with perfect seeing conditions are marked.

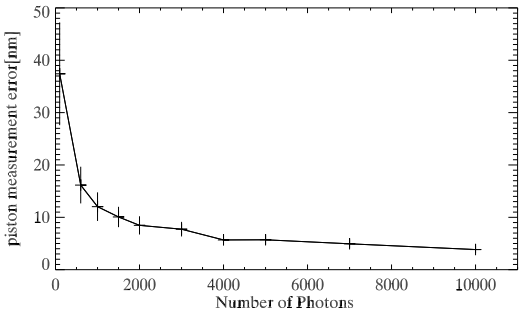

Figure 10. Rms measurement precision of the peak ratio technique under various photon noise conditions (λ=650nm).

where ν is the density of stars brighter than magnitude M per deg^2 in the considered region. This star density can be obtained from models of the galaxy or from measurements using for example the Guide Star Catalog, which has been employed here. From the results shown in Tabl. 1, it can be seen that a minimum accessible field of view of 10 arcminutes diameter is required to ensure accurate piston measurements at all times. This is comparable to the FOV of OWL.

3.4. Performance as Function of Telescope Size/Number of Segments

So far we have restricted our discussion on the determination of a single intersegment piston step. For the whole mirror made up of $\mathrm{N}_{segments}$ hexagonal segments with one subaperture on each side there will be $\mathrm{N}_{subapertures} < 3\mathrm{N}_{segments}$. The exact value of $\mathrm{N}_{subapertures}$ depends on mirror design aspects such as the outer shape and the central obscuration, since segments on the outer or inner borders have less than 6 neighbors. Each segment piston is determined by (up to) 6 piston step measurements and affects the segment piston measurements of all of its neighbors and hence of the whole mirror. This can be expressed mathematically as a system of linear equations of the form

$$\begin{aligned} \mathrm{Piston1}_i - \mathrm{Piston2}_i &= \mathrm{PS}_i, \\ i &= 1, ..., N_{subapertures}, \end{aligned} \tag{5}$$

where $\mathrm{Piston1}_i$ and $\mathrm{Piston2}_i$ are the Piston values of the two segments corresponding to subaperture i and PS_i is the measured piston step. Since the absolute average phase of the mirror is not of interest, it makes sense to keep it constant, adding a further constraint:

$$\sum_{j=1}^{N_{segments}} \mathrm{Piston} = 0. \tag{6}$$

Eqs. (5) and (6) constitute a simple linear system of $\mathrm{N}_{subapertures} + 1$ equations with $\mathrm{N}_{segments}$ unknowns (PS_i). At the Keck telescopes the technique of singular value decomposition (SVD) is used to solve this system (Chanan, 1998). We used this method on simulations of mirrors having up to 1000 segments and found it powerful and robust even on the scale of ELTs. Figures 11 and 12 show the results of some example simulations of mirrors of different sizes.

Table 1. Limiting stellar magnitude and the corresponding required accessible field (FOV) to find such a star with a probability of 90% for the peak ratio method at different photon levels at the North and South Galactic Poles. The given precision is the standard deviation of a piston step measurement at otherwise perfect conditions.

N_γ	Precision	Magnitude	FOV_{NGP} [arcmin]	FOV_{SGP} [arcmin]
10000	5 nm	11.8	10.1	8.0
2000	10 nm	13.7	5.4	4.7

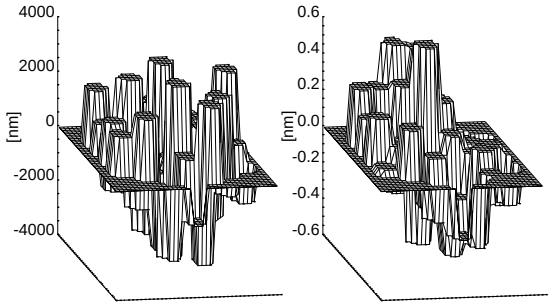

Figure 11. Segmented mirror of the Keck/GTC type (36 segments) before (left) and after (right) one phasing iteration. In this simulation perfect conditions were assumed. The original piston values are uniformly distributed with a range of 6530nm and a rms of 1990nm. Two measurements at different wavelengths have been performed (λ = 650nm, 850nm). The resulting rms piston error is 0.27nm, the rms piston step measurement error is 0.31nm.

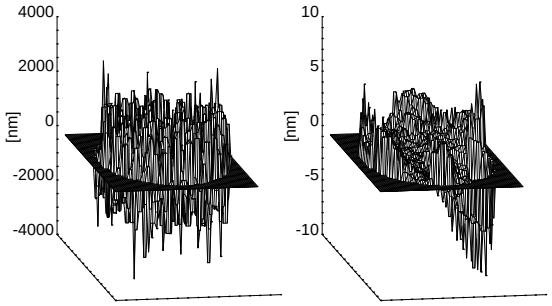

Figure 12. Segmented ELT mirror (846 segments) before (left) and after (right) one phasing iteration. In this simulation perfect conditions were assumed. The original piston values are uniformly distributed with a range of 4000nm and a rms of 1125nm. Two measurements at different wavelengths have been performed (λ = 650nm, 850nm). The resulting rms piston error is 2.0nm, the rms piston step measurement error is 0.4nm. The smooth residual is an example of the propagation of errors for which the sensitivity of the technique is low.

In the SVD method, one essentially provides a matrix, A, defined by the left hand side of Eqs. (5) and (6), and a vector defined by the right hand side, and SVD returns a vector of piston values. In the process, a pseudo-inverse of A (of $N_{subapertures}$ rows and $N_{segments}$ columns) is constructed that defines the linear system. Since we deal with an over-determined system, having more equations than unknowns, and furthermore our measured values are not perfect, SVD provides a best fit (in the sense of least-squares) to the set of data.

The measured data can be weighted to ensure that the piston step measurements with high precision will have more influence than those with less precision. This is done by simply dividing all equations i by the absolute error of the piston step measurement $\sigma(PS_i)$. Furthermore, piston step measurements for which the gaussian fit procedure appearantly did not find a valid solution can be excluded by making the corresponding line of the SVD matrix equal to zero. The same procedure should be applied if in a two-wavelength measurement a certain piston step measurement yields an ambiguous solution. Alternatively, the more probable solution can be chosen, and the corresponding error set to a high value to reflect the ambiguity. Applying these corrections to the straight forward implementation of SVD will give better results and furthermore will substantially enhance the robustness of the method. If weighting is not applied then a single erroneous or high-error piston step measurement can not only lead to a wrong piston estimation for the two corresponding segments, but can also affect a large number of their neighbors. In the worst case, it will not be possible to phase any of the segments. In the case of ELTs with hundreds or thousands of segments there is a high probability that there will be some faulty piston step measurements. Applying these weightings will provide stable results even in the presence of seeing and photon noise.

There are further possibilities to enhance the performance of the SVD procedure that should be used when applying on ELTs. First, a large number of subapertures leads to accumulating roundoff errors. The overall precision of the phasing procedure could be enhanced by iterative improvements of the solution to the linear equations. Second, a large number of subapertures means a large matrix A in the SVD calculations. One can save computation time and memory space by using the fact that we deal with a sparse linear system – A is mainly made up of zeroes that should not be processed and occupy memory. The computation times we find with the current, unoptimized code, indicate a computation time of the order of seconds when implemented on ELTs, if faster CPUs and parallel processing are employed. For further discussion of SVD as well as the code, see (Press, 1992).

3.5. Practical Aspects

It is clear that for this technique, the number of subapertures increases with the number of segments. If we consider a regular grid of hexagonal lenslets mapped onto an image of the segmented mirror, then in order to measure the piston step at each segment edge we need to map at least 2N+1 lenslets onto N segments. There is an extra lenslet centered on each segment, which can be used to measure tip-tilt. In the case of the OWL telescope, there are 64 segments on its longest axis and the corresponding number of subapertures is 129. If the hexagonal edge length of the lenslets is 0.3mm then the

length of the lenslet array would be 67mm, and the corresponding pupil demagnification would be approximately 1700. The lenslets used for phasing would be masked, leaving a 70 micron subaperture at the center. The lenslet array has to be precisely aligned to the image of the primary mirror for the Chanan technique to work. The alignment should at least be better than the size of the gaps between the segments. An alignment accuracy of 1mm referenced to the primary mirror would imply aligning the lenslet array to better than 0.6 microns. These specifications can be met with currently available technology. The alignment accuracy can be relaxed by including 'cross-hairs' in the lenslet masking, with the cross-hairs aligned to the segment edges. These cross-hairs can also relax the requirements on distortion in the pupil imaging; pupil distortion may be difficult to reduce when a large pupil demagnification is required. The drawback is a reduction in the light-gathering area of the subaperture. This can be compensated to some extent by elongating the subaperture in the direction perpendicular to the segment edges. This idea is implemented in the GTC where rectangular apertures are used for the phasing.

Another point to consider is the detector size. In order to avoid overlap, the field of view of the images given by the rectangular subapertures must be at least 5σ, where σ is the rms motion due to seeing.

$$\sigma^2 = 0.348(\lambda/d)^{1/3}(\lambda/r_0)^{5/3} \tag{7}$$

where λ is the wavelength, r_0 is the Fried parameter and d is the subaperture size. We will have N+1 images on the detector. Supposing a wavelength of 650nm, the size of the rectangular subapertures as 12cm, the number of images on the detector in one dimension as 65, and supposing a scale of 0.2"/pixel, then a detector of 1024x1024 pixels will be enough if the seeing is not bigger than 0.9" (r_0=14.5cm). In this case every image is within a square window of side 3.2" (16 pixels). If the seeing is worse then a 2048x2048 pixels detector will be necessary. Again, this technology is currently available.

4. CONCLUSIONS AND PLANS

The phasing techniques addressed in this article have been tentatively reviewed for their potential accuracy. We so far investigated in detail the Chanan narrow-band technique. We showed that a modified version of it can work with sufficient precision and is feasible on telescopes as large as 100m. A comparison of the original Chanan technique and the alternatively developed peak ratio technique showed substantial performance improvements of the latter.

Much work still lies ahead before completing an extensive assessment, which will have to take into account a complete and representative set of error sources. So far we have assumed that phasing is dealt with the same way as it is done in the Keck telescopes i.e., closed-loop phasing with position sensors, the techniques described in this article being used for calibration of the sensors. An alternative could be on-sky, closed loop phasing i.e. a scheme that would make phasing an integral part of wavefront control as it is done in active telescopes, thereby providing higher reliability and full transparency. Whether such approach is feasible at all is yet unknown; the key issues to be addressed will not only deal with accuracy, but also with the limiting magnitude of the reference source(s) and the implied sky coverage, the affordable integration time in relation to the stability of segments phase errors, and the interface with adaptive optics. In particular, any technique that would require prior adaptive correction of atmospheric turbulence will necessarily reduce the field available for suitable phasing references. On the other hand, piston and tilt detection prior to adaptive correction will most likely require short exposure or rely on sub-aperture measurements (the size of the sub-apertures being comparable to atmospheric coherence length), thereby implying brighter sources and limited sky coverage.

ACKNOWLEDGMENTS

This research has benefited from the support of the European Commission RTN program: "Adaptive Optics for Extremely Large Telescopes", contract #HPRN-CT-2000-00147.

REFERENCES

J. Arasa, F. Laguarta, C. Pizarro, N. Tomas, A. Pinto, *Design of an interferometric system for piston measurements in segmented primary mirrors*, Proc. SPIE, 4093, 397-406, 2000

C. D. Bello Figueroa, *Improving the image quality of large segmented mirror telescopes* PhD thesis, Instituto de Astrofísica de Canarias, La Laguna, Tenerife, 2000

C. D. Bello, N. Devaney, J. Castro, *The effect of piston errors on the image quality of ground-based segmented mirror telescopes*, Rev. Mex. Astron. Astrofis., 36,57-66, 2000

G. Chanan, M. Troy, F. Dekens, S. Michaels, J. Mast, D. Kirkman, *Phasing the mirror segments of the Keck telescopes: the broadband phasing algorithm*, App.Opt., Vol. 37 (1), 140-155, 1998

G. Chanan, M. Troy, C. Ohara, *Phasing the Primary Mirror Segments of the Keck Telescopes: A comparison of Different Techniques*, Proc. SPIE 4003, 188-201, 2000

S. Cuevas, V.G. Orlov, F. Garfias, V.V. Voitsekhovich, L. Sanchez, *Curvature equation for a segmented telescope*, Proc. SPIE, 4003,291-302, 2000

N. Devaney, L. Cavaller, L. Jochum, C.D. Bello, J. Castro, *Guacamole: The GTC Guiding, Acquisition and Calibration Module*, Proc. SPIE, 4003, 146-153, 2000

K. Dohlen, F. Decertiat, F. Fresneau, P. Lanzoni, *A dual wavelength random phaseshift interferometer for phasing large segmented primaries*, Proc. SPIE, 3352, 551, 1998

D. Gavel, *The effect of the Keck Telescope's Segmented Primary on the Performance of the Keck Adaptive Optics System*, Proc. SPIE, 3126, 144-150, 1997

A.D. Glecker, K.P. Pflibsen, B.L. Ulich, D.D. Smith, *Surface control techniques for the segmented primary mirror in the Large Lunar Telescope*, Proc. SPIE, 1494, 454-471, 1991

R. Horton, E. Huber, L. Bernotas, L. Yee, A. Roberts, J. Norton, E. Corbett, R. Humphries, *Absolute piston phasing of segmented-mirror optical systems using depth-modulated white-light interferometry*, Proc. SPIE, 1236, P974, 1990

B. Jacobsen and R. Angel, *High accuracy wavefront stellar wavefront sensing using a Zernike interferometer*, Bull. American Astron. Soc., 26, p1373, 1994

M.G. Lofdahl, R.L. Kendrick, A. Harwit, K.E. Mitvhell, A.L. Duncan, J.H. Seldin, R.G. Paxman, D.S. Acton, *A Phase Diversity Experiment to Measure Piston Misalignment on the Segmented Primary Mirror of the Keck II Telescope*, Proc. SPIE, 3356, 1190-1201, 1998

R.H. Minor et al., *Displacement sensors for the primary mirror of the W.M. Keck telescope*, Proc. SPIE, 1236, 1990

J. Nelson and T. Mast, *Giant Optical Devices*, Proc. Backaskog Workshop on Extremely Large Telescopes, 1-11, 1999

M. Owner-Petersen and T. Andersen, *Overview of Optical Metrology for Segment Phasing*, Proc. Backaskog Workshop on Extremely Large Telescopes, 152-161, 1999

R.G. Paxman and J.R. Fienup, *Optical misalignment sensing and image reconstruction using phase diversity*, J.Opt.Soc.Am. A, 5, 914-922,1988

W.H. Press, B.P. Flannery, S.A. Teukolsky, W.T. Vetterling, *Numerical Recipes in C: the art of scientific computing*, Cambridge U. Press, New York, 32-70, 1992

F. Roddier, M. Northcott, J.E. Graves, *A simple low-order Adaptive Optics system for Near-Infrared applications*, PASP, 103, 131-149, 1991

J.M Rodriguez-Ramos and J.J Fuensalida, *Piston Detection of a Segmented Mirror Telescope using a Curvature Sensor. Preliminary Results with Numerical Simulations*, Proc. SPIE 2871, 613-616, 1996

N. Yaitskova & K. Dohlen, *Simulation of imaging performance for extremely large segmented telescopes*, Proc. SPIE, 4003, 279-290

N. Yaitskova & K. Dohlen, *Theoretical and computational study of the image quality in extremely large segmented telescopes*, in preparation

G.W. Zeiders, E.E. Montgomery, *Diffraction Effects with Segmented Apertures*, Proc. SPIE, 3356, 799-809, 1998